Geophysical Journal (1988) **94**, 387–397

Application of the modified Cagniard technique to transient electromagnetic diffusion problems

A. T. de Hoop*
Schlumberger Doll Research, Old Quarry Road, Ridgefield, Connecticut 06877-4108, *USA*

M. L. Oristaglio†
Etudes et Productions Schlumberger, 26, rue de la Cavée Clamart 92140, *France*

Accepted 1988 February 14. Received 1988 February 1; in original form 1987 July 13

SUMMARY

A version of Cagniard's technique for inverting integral transforms is adapted to diffusion problems and illustrated with the 2-D example of two semi-infinite media of different electrical conductivity excited by a transient line-source of electric current at their interface. The field equations are first solved in the transform domain, i.e. following a Laplace transformation with respect to time (with real, positive transform parameter) and a Fourier transformation with respect to the spatial coordinate parallel to the interface. Deformation of the path of integration for the inverse Fourier transformation allows the inverse Laplace transformation to be obtained by inspection. The electromagnetic field at any point in the configuration can then be obtained by numerical evaluation of well-behaved integrals. In the more diffusive half-space, there is a single integral to be evaluated, whereas in the less diffusive domain, there are two: one corresponding to the direct 'wave', the other to a diffusive 'head wave' which develops along the interface and influences certain regions of space–time.

Key words: electromagnetic diffusion, modified Cagniard method, plane-layered media

1 INTRODUCTION

Insight into the behaviour of transient electromagnetic fields in conductive structures is important when interpreting data acquired in electromagnetic exploration for minerals or groundwater. For complex structures, only numerical methods—such as the finite-difference method (Oristaglio & Hohmann 1984; Goldman & Stoyer 1983) or finite-element method (Kuo & Cho 1980)—have sufficient flexibility to give quantitative results for the field values. But for simple structures, like plane-layered models, analytical results can be obtained that, apart from serving to check numerical results, can have considerable interest of their own. An example is the 'smoke-ring' model introduced by Nabighian (1979), which provides a simple, intuitive picture of the transient currents induced in a half-space by a current loop source at the surface.

The present paper develops an analytical method for transient electromagnetic diffusion through plane-layered media. The method employs ideas that have been successfully used to study the propagation of impulsive waves in layered media, where it is called the 'modified Cagniard' or 'Cagniard–de Hoop' technique (de Hoop 1960, 1961, 1979; de Hoop & van der Hijden 1983, 1984; see also Achenbach 1973; Aki & Richards 1980). The method is illustrated for a two-media configuration with a plane boundary, where each medium is characterized by a constant conductivity and a constant permeability. An impulsive line current is located at the boundary and generates a 2-D diffusive electromagnetic field. Recently, such a model has been used to study the behaviour of underwater transient electromagnetic systems for mapping sea-floor conductivity (Edwards & Cheesman 1987). It has also been used to study the propagation of electromagnetic signals generated by cables lying on the sea-floor (see Inan, Fraser-Smith & Villard 1986 for a recent discussion of this work, which has concentrated on the frequency response of the model). Our main purpose here is to use the model as a canonical example of Cagniard's method applied to transient diffusion problems. Of particular interest is the physical insight provided by this method: at each point in the configuration, the transient field is decomposed exactly into physically meaningful parts, each of which is given by a simple, well-behaved integral.

* On leave from Delft University of Technology, Department of Electrical Engineering, Laboratory of Electromagnetic Research, The Netherlands.
† Present address: Schlumberger, Austin Systems Center, 8311 N. FM 620 Rd, PO Box 200015, Austin, Texas 78720-0015 USA.

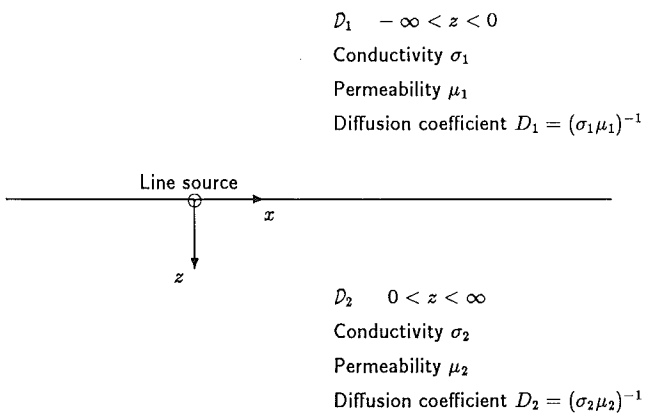

Figure 1. Geometry of the problem.

2 DESCRIPTION OF THE CONFIGURATION

We consider the transient electromagnetic fields in a medium with a plane interface separating two half-spaces (Fig. 1). Each half-space is homogeneous and isotropic, with constant conductivity σ and permeability μ. We assume that displacement currents contribute negligibly to the electromagnetic field and thus ignore the permittivity ϵ of each medium. Position in the configuration is specified by coordinates (x, y, z) with respect to a Cartesian reference frame. The z-axis is normal to the interface, while the y-axis is directed along the line current, i.e. perpendicular to the 2-D cross-section shown in Fig. 1. The strength of the line current is assumed to be independent of y, giving a purely 2-D problem. Other properties of the configuration are summarized in the figure.

The time coordinate is denoted by t. It is assumed that the source starts to act at $t = 0$ and that, prior to this, the electromagnetic field is zero everywhere. In actual transient measurements (see e.g. McCracken, Oristaglio & Hohmann 1986), the current is usually switched off at $t = 0$ and one observes the decay of the field from its steady-state value. This case can be obtained from our analysis simply by subtracting the results from the steady–state value of the field components.

3 FIELD EQUATIONS

In a homogeneous, isotropic domain, the 2-D electromagnetic field that can be generated by a line-source current with volume density $\mathbf{J} = (0, J_y, 0)$ consists of an electric field with components $\mathbf{E} = (0, E_y, 0)$ and a magnetic field with components $\mathbf{H} = (H_x, 0, H_z)$. In the diffusive approximation (i.e. neglecting displacement currents), the field is governed by the following partial differential equations:

$$-\partial_x H_z + \partial_z H_x - \sigma E_y = J_y, \tag{1}$$

$$\partial_x E_y + \mu \partial_t H_z = 0, \tag{2}$$

$$-\partial_z E_y + \mu \partial_t H_x = 0. \tag{3}$$

The electric current source is now taken to be a line current located at $x = 0$, $z = 0$; thus, $J_y = I(t)\delta(x, z)$, where $I(t)$ is the current in the source and $\delta(x, z)$ is the 2-D (spatial) delta function. The action of the source can be accounted for by the following boundary conditions, which follow from integrating (1) and (3) over an arbitrarily small interval around $z = 0$ and using the properties of the delta function,

$$\lim_{z\downarrow 0} H_x - \lim_{z\uparrow 0} H_x = I(t)\delta(x) \tag{4}$$

$$\lim_{z\downarrow 0} E_y - \lim_{z\uparrow 0} E_y = 0, \tag{5}$$

where $z\downarrow 0$ and $z\uparrow 0$ indicate one-sided limits as z approaches 0 from positive and negative values, respectively.

4 METHOD OF SOLUTION

4.1 Transform domain

In our method of solution, we first calculate the field quantities in the 'transform' domain. To this end, we carry out a one-sided Laplace transformation with respect to time with real, positive transform parameter s (this is, in fact, the easiest way to take into account causality). We then perform a Fourier transformation with respect to x, the coordinate parallel to the boundary, with transform parameter $s^{1/2}\alpha$. This choice of transform parameter for the Fourier transformation is designed to facilitate the transformation back to the space–time domain by the modified Cagniard method. To show the notation, we write down the relevant transformations for the electric field:

$$\hat{E}_y(x, z, s) = \int_0^\infty \exp(-st) E_y(x, z, t)\, dt, \tag{6}$$

$$\tilde{E}_y(\alpha, z, s) = \int_{-\infty}^\infty \exp(is^{1/2}\alpha x)\hat{E}_y(x, z, s)\, dx. \tag{7}$$

Using Fourier's inversion theorem, we also have

$$\hat{E}_y(x, z, s) = s^{1/2}/2\pi \int_{-\infty}^\infty \exp(-is^{1/2}\alpha x)\tilde{E}_y(\alpha, z, s)\, d\alpha, \tag{8}$$

where we have taken into account that the transform parameter is $s^{1/2}\alpha$.

Application of these transformations to the field equations (1)–(3) leads to the following transform-domain equations, which include the initial conditions and continuity of the field quantities as a function of x and hold when $z \neq 0$:

$$is^{1/2}\alpha\tilde{H}_z + \partial_z\tilde{H}_x - \sigma\tilde{E}_y = 0, \tag{9}$$

$$-is^{1/2}\alpha\tilde{E}_y + s\mu\tilde{H}_z = 0, \tag{10}$$

$$-\partial_z\tilde{E}_y + s\mu\tilde{H}_x = 0. \tag{11}$$

Elimination of $\tilde{H}_z$ from this system gives the equations

$$\partial_z\tilde{H}_x = \mu^{-1}(\alpha^2 + D^{-1})\tilde{E}_y, \tag{12}$$

$$\partial_z\tilde{E}_y = s\mu\tilde{H}_x, \tag{13}$$

where

$$D = 1/\sigma\mu \tag{14}$$

is the diffusion coefficient. Furthermore, the boundary

conditions in the transform domain become

$$\lim_{z\downarrow 0} \tilde{H}_x - \lim_{z\uparrow 0} \tilde{H}_x = \hat{I}, \tag{15}$$

$$\lim_{z\downarrow 0} \tilde{E}_y - \lim_{z\uparrow 0} \tilde{E}_y = 0, \tag{16}$$

where $\hat{I}$ is the Laplace transform of the source current.

In what follows, we distinguish the field quantities in the two half-spaces by the superscripts (1) for the upper half-space and (2) for the lower half-space. From equations (12) and (13), it follows that the solution in the upper half-space that is bounded as $z \rightarrow -\infty$ is

$$\tilde{E}_y^{(1)} = -s^{1/2}\hat{I}A_1 \exp(s^{1/2}\gamma_1 z), \tag{17}$$

$$\tilde{H}_x^{(1)} = -(\gamma_1/\mu_1)\hat{I}A_1 \exp(s^{1/2}\gamma_1 z), \tag{18}$$

where

$$\gamma_1 = (\alpha^2 + D_1^{-1})^{1/2} > 0. \tag{19}$$

In the lower half-space, the solution that is bounded as $z \rightarrow \infty$ is

$$\tilde{E}_y^{(2)} = -s^{1/2}\hat{I}A_2 \exp(-s^{1/2}\gamma_2 z), \tag{20}$$

$$\tilde{H}_x^{(2)} = (\gamma_2/\mu_2)\hat{I}A_2 \exp(-s^{1/2}\gamma_2 z), \tag{21}$$

where

$$\gamma_2 = (\alpha^2 + D_2^{-1})^{1/2} > 0. \tag{22}$$

The constants A_1 and A_2 are obtained by imposing the boundary conditions (15) and (16); we find

$$A_1 = A_2 = \frac{1}{\gamma_1/\mu_1 + \gamma_2/\mu_2} = \frac{\mu_1\mu_2}{\mu_2\gamma_1 + \mu_1\gamma_2} \equiv A. \tag{23}$$

Note that A does not depend on the Laplace transform parameter s.

This completes the solution of the relevant equations in the transform domain. Subsequent sections describe the transformation back to the space–time domain using the modified Cagniard method and are followed by numerical examples.

4.2 Back to the space–time domain

To return to the space–time domain, we must invert the Laplace and Fourier transformations that were used to obtain equations (17)–(23). Symbolically, we can write for a typical field component, for example, $E_y^{(1)}$,

$$E_y^{(1)}(x, z, t) = \mathscr{L}^{-1}\{\mathscr{F}^{-1}\{\tilde{E}_y^{(1)}(\alpha, z, s)\}\}, \tag{24}$$

where $\mathscr{L}^{-1}\{\ \}$ and $\mathscr{F}^{-1}\{\ \}$ indicate, respectively, the inverse Laplace and Fourier transformations of the quantities in braces.

The essence of the modified Cagniard method for obtaining space–time results from the two inverse transformations is to deform the path of integration of the inverse Fourier transformation in the complex plane until the integral resembles the *forward* Laplace transformation of a well-behaved function, with a real, positive 'time' parameter defined along the path. In problems of 2-D *wave* propagation, the inverse Laplace and Fourier transformations cancel perfectly after the contour deformation, yielding algebraic expressions for the simplest time response. In a 3-D problem, a single finite-range integral remains after cancellation of the inverse transformations. We follow a similar procedure for inverting the transformations in the diffusion problem. The main difference between the diffusion and wave problems is that, in a 2-D diffusion problem, a single integral remains to be evaluated even for the simplest time response.

We illustrate this procedure by considering in detail the solution for the field component E_y. We shall assume that $\sigma_1\mu_1 < \sigma_2\mu_2$ and, hence $D_1 > D_2$. The case of vanishing conductivity (air over a conducting half-space) follows by taking the limit as the conductivity goes to zero through positive values. We compute the solution for a (unit) step-function current source, so that

$$\hat{I} = 1/s. \tag{25}$$

Consider first the expression for the field in the more diffusive domain $\mathscr{D}_1$. On comparing (8), (17) and (25), we obtain for the inverse Fourier transformation in (24),

$$\hat{E}_y^{(1)}(x, z, s) = -\frac{1}{2\pi}\int_{-\infty}^{\infty} \exp[-s^{1/2}(i\alpha x + \gamma_1 |z|)]A(\alpha)\, d\alpha, \tag{26}$$

in which A is given by (23). Note that we are not using a special symbol to indicate that $\hat{E}_y^{(1)}(x, z, s)$ is the step-response of the system; furthermore, in the expressions that follow, we will omit the arguments of this function and write $\hat{E}_y^{(1)}$ in place of $\hat{E}_y^{(1)}(x, z, s)$.

The first step in the evaluation of $\hat{E}_y^{(1)}$ is to introduce p as the variable of integration, by the substitution $p = i\alpha$. Equation (26) becomes

$$\hat{E}_y^{(1)} = -\frac{1}{2\pi i}\int_{-i\infty}^{i\infty} \exp[-s^{1/2}(px + \bar{\gamma}_1 |z|)]\bar{A}(p)\, dp, \tag{27}$$

where the bar over a symbol indicates the relevant replacement. For example,

$$\bar{\gamma}_1 = (D_1^{-1} - p^2)^{1/2}. \tag{28}$$

Next, the integrand in the above equation is continued analytically into the complex p-plane, with the aim of deforming the path of integration in (27) into a path where

$$px + \bar{\gamma}_1 |z| = \kappa, \tag{29}$$

with κ real and positive. In this process, we keep both $\mathrm{Re}(\bar{\gamma}_1) > 0$ and $\mathrm{Re}(\bar{\gamma}_2) > 0$. To do this, branch cuts are introduced along

$$\mathrm{Im}(p) = 0 \qquad D_1^{-1/2} < |\mathrm{Re}(p)| < \infty, \quad \text{and}$$

$$\mathrm{Im}(p) = 0 \qquad D_2^{-1/2} < |\mathrm{Re}(p)| < \infty.$$

In the cut p-plane, the integrand is then single-valued and free from singularities. It is also real-valued when

$$\mathrm{Im}(p) = 0 \qquad -D_1^{-1/2} < \mathrm{Re}(p) < D_1^{-1/2}.$$

With the above conditions, Schwarz's reflection principle applies to the integrand which thus takes on complex conjugate values at conjugate complex points in the p-plane.

In wave-propagation problems, the paths in the complex plane that satisfy (29) as continuous deformations of the imaginary p-axis are called 'modified Cagniard' paths. Solving for p in this equation, we find that the appropriate

path is given by two complex conjugate branches (Fig. 2), $p = p_1$ and $p = p_1^*$, where

$$p_1 = \kappa \frac{x}{r^2} + i(\kappa^2 - \kappa_1^2)^{1/2} \frac{|z|}{r^2} \quad \text{with} \quad \kappa_1 < \kappa < \infty, \tag{30}$$

in which

$$r = (x^2 + z^2)^{1/2}, \tag{31}$$

$$\kappa_1 = r/D_1^{1/2}. \tag{32}$$

The hyperbolic path composed of $p = p_1$ and $p = p_1^*$ is symmetric with respect to the real p-axis. It crosses the axis at $p = x/rD_1^{1/2}$ when $\kappa = \kappa_1$, i.e. between the branch points $-D_1^{1/2}$ and $+D_1^{1/2}$ (Fig. 2).

When the original integration path along the imaginary p-axis is joined to the modified Cagniard path with circular arcs at infinity, the contribution to the integral from the circular arcs vanishes (Jordan's lemma) because

$$|\bar{A} \exp(-s^{1/2}\bar{\gamma}_1 |z|)| \to 0 \quad \text{as} \quad p \to \infty$$

(recall that s is real and positive and the real part of $\bar{\gamma}_1$ was kept positive by the choice of branch cuts). By Cauchy's theorem, the expression for $\hat{E}_y^{(1)}$ can thus be rewritten as

$$\hat{E}_y^{(1)} = -\frac{1}{\pi} \int_{\kappa_1}^{\infty} \exp(-s^{1/2}\kappa) \operatorname{Im}(\bar{A} \partial_\kappa p_1)\, d\kappa. \tag{33}$$

In (33), κ has been introduced as the variable of integration using (30). Moreover, the property that both s and κ are real has been used, along with the fact that the integrand has complex-conjugate values along the paths $p = p_1$ and $p = p_1^*$. The integration along the conjugate paths can thus be combined into the single integral (33). Along the path of integration in (33), we have

$$\bar{\gamma}_1 = \kappa \frac{|z|}{r^2} - i(\kappa^2 - \kappa_1^2)^{1/2} \frac{x}{r^2} \quad \text{with} \quad \kappa_1 < \kappa < \infty, \tag{34}$$

while the Jacobian $\partial_\kappa p_1$ is given by

$$\partial_\kappa p_1 = \frac{i\bar{\gamma}_1}{(\kappa^2 - \kappa_1^2)^{1/2}}. \tag{35}$$

With these substitutions, the inverse Fourier transformation is now in a form where the Laplace inversion integral in (24) can be moved inside the κ integral. We observe that $\exp(-s^{1/2}\kappa)$ is the Laplace transform of the causal time function

$$G(t, \kappa) = H(t) \frac{\kappa}{(4\pi t^3)^{1/2}} \exp(-\kappa^2/4t), \tag{36}$$

where $H(t)$ is the Heaviside step-function and $\kappa > 0$. The final space–time expression for $E_y^{(1)}(x, z, t)$ is then

$$E_y^{(1)}(x, z, t) = -\frac{1}{\pi} \int_{\kappa_1}^{\infty} G(t, \kappa) \operatorname{Im}(\bar{A} \partial_\kappa p_1)\, d\kappa. \tag{37}$$

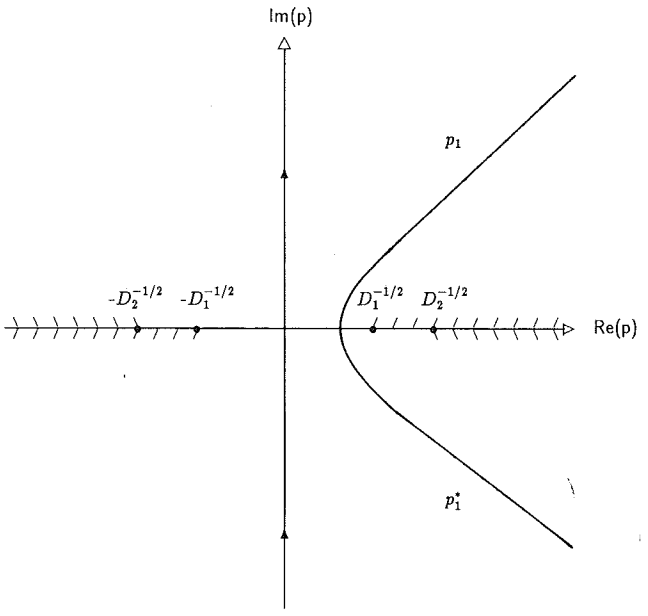

Figure 2. Modified Cagniard path in the complex p-plane for calculating the response in the more diffusive domain $\mathcal{D}_1$. p_1 and p_1^* are the complex conjugate limbs of the hyperbolic path. The path crosses the real p-axis at a point between the branch cuts originating at $\pm D_1^{-1/2}$.

4.3 Diffusive head waves

The solution for the electric field $E_y^{(2)}$ in the less diffusive domain $\mathcal{D}_2$ follows closely the derivation in the previous section on replacing $\bar{\gamma}_1$ by $\bar{\gamma}_2$ in (27). In this domain, however, a new phenomenon arises. The modified Cagniard path along which the final integration is taken can intersect a branch cut on the real p-axis. The appropriate loop integral around the branch cut, which must be added to keep the integrand single-valued, adds a diffusive 'head-wave' contribution to the field in certain regions of space–time. These regions depend on the distance of the receiver from the source and on the contrast in material properties across the interface.

We start with the inverse Fourier integral for $\hat{E}_y^{(2)}$, after the substitution $p = i\alpha$,

$$\hat{E}_y^{(2)} = -\frac{1}{2\pi i} \int_{-i\infty}^{i\infty} \exp[-s^{1/2}(px + \bar{\gamma}_2 z)] \bar{A}(p)\, dp, \tag{38}$$

where

$$\bar{\gamma}_2 = (D_2^{-1} - p^2)^{1/2}, \tag{39}$$

and the absolute value signs on z have been dropped since $z > 0$ in $\mathcal{D}_2$. In the region of observation

$$0 \le |x|/r \le (D_2/D_1)^{1/2}, \tag{40}$$

the appropriate modified Cagniard path consists of $p = p_2$ and $p = p_2^*$, where

$$p_2 = \kappa \frac{x}{r^2} + i(\kappa^2 - \kappa_2^2)^{1/2} \frac{z}{r^2} \quad \text{with} \quad \kappa_2 < \kappa < \infty. \tag{41}$$

and

$$\kappa_2 = r/D_2^{1/2}. \tag{42}$$

The hyperbolic path composed of $p = p_2$ and $p = p_2^*$ is again symmetric with respect to the real p-axis and crosses the axis at $p = x/rD_2^{1/2}$ when $\kappa = \kappa_2$. In the region of observation (40), the point of intersection of the new path and the real

p-axis still lies between the branch points $-D_1^{1/2}$ and $+D_1^{1/2}$. The path deformation is thus complete and the final space–time expression for $E_y^{(2)}$ in this region is simply

$$E_y^{(2)}(x, z, t) = -\frac{1}{\pi}\int_{\kappa_2}^{\infty} G(t, \kappa)\,\mathrm{Im}\,(\bar{A}\partial_\kappa p_2)\,d\kappa. \tag{43}$$

The diffusive head wave occurs in the region of observation

$$(D_2/D_1)^{1/2} \le |x|/r \le 1. \tag{44}$$

Since the electric field is symmetric in x, we need only consider the region with x positive

$$(D_2/D_1)^{1/2} \le x/r \le 1. \tag{45}$$

Here, the modified Cagniard path composed of $p = p_2$ and $p = p_2^*$ (41) intersects the real p-axis at a point along the branch cut associated with $\bar{\gamma}_1$ (Fig. 3) and must be supplemented by a loop integral around the branch cut. Along this loop, too, we maintain the condition

$$px + \bar{\gamma}_2 |z| = \kappa, \tag{46}$$

with κ real and positive. The values of p that follow from (46) when considered along the loop are denoted as $p = p_{2,1}$ and $p = p_{2,1}^*$, where

$$p_{2,1} = \kappa\frac{x}{r^2} - (\kappa_2^2 - \kappa^2)^{1/2}\frac{z}{r^2} + i0 \quad \text{with} \quad \kappa_{2,1} < \kappa < \kappa_2. \tag{47}$$

and

$$\kappa_{2,1} = \frac{x}{D_1^{1/2}} + (D_2^{-1} - D_1^{-1})^{1/2} z. \tag{48}$$

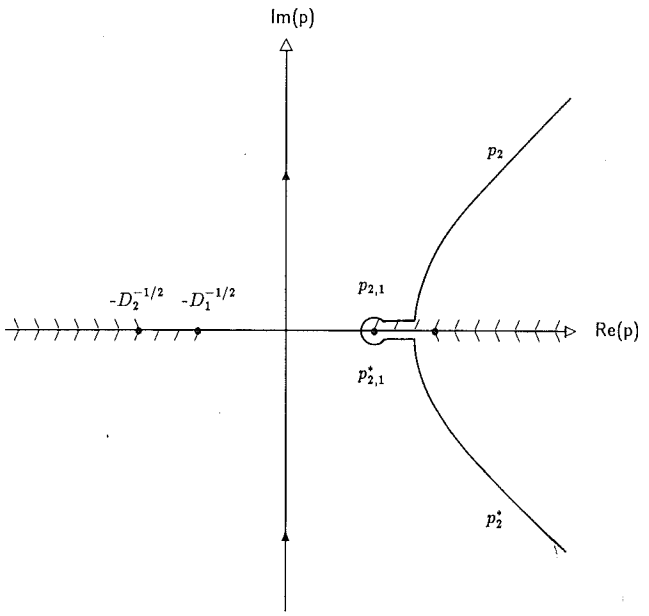

Figure 3. Modified Cagniard path in the complex p-plane for calculating the response in the less diffusive domain $\mathcal{D}_2$ in the region where the diffusive head wave is present. The hyperbolic path composed of p_2 and p_2^* intersects the real p-axis at a point between the branch cuts originating at $D_1^{-1/2}$ and $D_2^{-1/2}$ and must be supplemented by a loop around the branch cut (the paths $p_{2,1}$ and $p_{2,1}^*$).

Along $p = p_{2,1}$, we also have

$$\bar{\gamma}_2 = \kappa\frac{z}{r^2} + (\kappa_2^2 - \kappa^2)^{1/2}\frac{x}{r^2}. \tag{49}$$

and

$$\partial_\kappa p_{2,1} = \frac{\bar{\gamma}_2}{(\kappa_2^2 - \kappa^2)^{1/2}}. \tag{50}$$

The final space–time expression for $E_y^{(2)}$ in this region is the sum of the contributions from the loop integral (the diffusive head wave) and the hyperbolic path (the direct wave),

$$E_y^{(2)}(x, z, t) = -\frac{1}{\pi}\int_{\kappa_{2,1}}^{\kappa_2} G(t, \kappa)\,\mathrm{Im}\,(\bar{A}\partial_\kappa p_{2,1})\,d\kappa - \frac{1}{\pi}\int_{\kappa_2}^{\infty} G(t, \kappa)\,\mathrm{Im}\,(\bar{A}\partial_\kappa p_2)\,d\kappa. \tag{51}$$

The diffusive head-wave field in (51) is similar to the lateral-wave field that King (1985) identified in the harmonic response of the two-half-space model to an electric dipole source. He made this interpretation after carefully deriving an approximate formula for the field from an exact integral expression. The decomposition of the transient field of the line source given by (51) involves no approximations.

5 MAGNETIC FIELDS

The magnetic fields in the two half-spaces follow directly from (18), (21) and contour deformations similar to those described above. We will just quote the results here. For the magnetic field in the more diffusive domain $\mathcal{D}_1$, we have

$$H_x^{(1)}(x, z, t) = -\frac{1}{\pi}\int_{\kappa_1}^{\infty} F(t, \kappa)\,\mathrm{Im}\,(\bar{\gamma}_1\mu_1^{-1}\bar{A}\partial_\kappa p_1)\,d\kappa, \tag{52}$$

$$H_z^{(1)}(x, z, t) = -\frac{1}{\pi}\int_{\kappa_1}^{\infty} F(t, \kappa)\,\mathrm{Im}\,(p_1\mu_1^{-1}\bar{A}\partial_\kappa p_1)\,d\kappa, \tag{53}$$

where $F(t, \kappa)$ is the causal time function

$$F(t, \kappa) = H(t)\frac{1}{(\pi t)^{1/2}}\exp(-\kappa^2/4t), \tag{54}$$

and where the integration is over the modified Cagniard path described by (30). In deriving these expressions, we used the fact that F is the inverse Laplace transform of the function $s^{-1/2}\exp(-s^{1/2}\kappa)$.

For the magnetic field in the less diffusive domain $\mathcal{D}_2$, we have in the region of observation (40),

$$H_x^{(2)}(x, z, t) = \frac{1}{\pi}\int_{\kappa_2}^{\infty} F(t, \kappa)\,\mathrm{Im}\,(\bar{\gamma}_2\mu_2^{-1}\bar{A}\partial_\kappa p_2)\,d\kappa. \tag{55}$$

and

$$H_z^{(2)}(x, z, t) = -\frac{1}{\pi}\int_{\kappa_2}^{\infty} F(t, \kappa)\,\mathrm{Im}\,(p_2\mu_2^{-1}\bar{A}\partial_\kappa p_2)\,d\kappa. \tag{56}$$

In the region of observation (45), the expressions for H are supplemented by the head-wave contribution, giving

$$H_x^{(2)}(x, z, t) = \frac{1}{\pi}\int_{\kappa_{2,1}}^{\kappa_2} F(t, \kappa)\,\mathrm{Im}\,(\bar{\gamma}_2\mu_2^{-1}\bar{A}\partial_\kappa p_{2,1})\,d\kappa + \frac{1}{\pi}\int_{\kappa_2}^{\infty} F(t, \kappa)\,\mathrm{Im}\,(\bar{\gamma}_2\mu_2^{-1}\bar{A}\partial_\kappa p_2)\,d\kappa, \tag{57}$$

and

$$H_z^{(2)}(x, z, t) = -\frac{1}{\pi}\int_{\kappa_{2,1}}^{\kappa_2} F(t, \kappa)\,\mathrm{Im}\,(p_{2,1}\mu_2^{-1}\bar{A}\partial_\kappa p_{2,1})\,d\kappa - \frac{1}{\pi}\int_{\kappa_2}^{\infty} F(t, \kappa)\,\mathrm{Im}\,(p_2\mu_2^{-1}\bar{A}\partial_\kappa p_2)\,d\kappa. \quad (58)$$

The integrals are taken over the appropriate paths described by (41) and (47).

6 THE FIELDS AT THE INTERFACE

Although the expressions given above are suitable for direct numerical evaluation (to be described in the next section), there are special cases in which they simplify somewhat and can lead to closed-form expressions for the fields. To reduce some of the 'symbol clutter' in the expressions that follow, we introduce time variables scaled by the appropriate diffusion constants,

$$T_1 = 4D_1 t = 4t/\sigma_1\mu_1,$$
$$T_2 = 4D_2 t = 4t/\sigma_2\mu_2.$$

The factor of 4 provides an additional scaling natural to 2-D diffusion.

Consider first the electric field E_y, which is continuous across the interface. Since E_y is an even function of x, we limit attention to $0 \le x < \infty$. With $z = 0$ and $x \ge 0$, the modified Cagniard path for equation (27) or (38) reduces to a loop around the branch cut associated with $\bar{\gamma}_1$ in the right half of the p-plane. We thus arrive at

$$E_y(x, z = 0, t) = -\frac{1}{\pi}\int_{D_1^{-1/2}}^{\infty} G(t, px)\,\mathrm{Im}\,[\bar{A}(p)]\,dp, \quad (59)$$

Where in the expression for $\bar{A}(p)$,

$$\bar{\gamma}_1 = -i(p^2 - D_1^{-1})^{1/2}, \quad (60)$$

and

$$\bar{\gamma}_2 = \begin{cases} (D_2^{-1} - p^2)^{1/2} & \text{if } D_1^{-1/2} < p < D_2^{-1/2}, \\ -i(p^2 - D_2^{-1})^{1/2} & \text{if } D_2^{-1/2} < p < \infty. \end{cases} \quad (61)$$

Now, in the region $D_1^{-1/2} < p < D_2^{-1/2}$, we have

$$\mathrm{Im}\,[\bar{A}(p)] = \frac{\mu_1\mu_2^2(p^2 - D_1^{-1})^{1/2}}{\mu_2^2(p^2 - D_1^{-1}) - \mu_1^2(p^2 - D_2^{-1})}, \quad (62)$$

whereas in the region $D_2^{-1/2} < p < \infty$,

$$\mathrm{Im}\,[\bar{A}(p)] = \frac{\mu_1\mu_2^2(p^2 - D_1^{-1})^{1/2} - \mu_2\mu_1^2(p^2 - D_2^{-1})^{1/2}}{\mu_2^2(p^2 - D_1^{-1}) - \mu_1^2(p^2 - D_2^{-1})}. \quad (63)$$

This last expression can only be used if the numerator and denominator have no common zeros, i.e. if $\mu_2 \ge \mu_1$. Splitting the integral into two parts, we can write

$$E_y(x, z = 0, t) = -\frac{1}{\pi}\int_{D_1^{-1/2}}^{\infty} G(t, px)\frac{\mu_1\mu_2^2(p^2 - D_1^{-1})^{1/2}}{\mu_2^2(p^2 - D_1^{-1}) - \mu_1^2(p^2 - D_2^{-1})}\,dp + \frac{1}{\pi}\int_{D_2^{-1/2}}^{\infty} G(t, px)\frac{\mu_2\mu_1^2(p^2 - D_2^{-1})^{1/2}}{\mu_2^2(p^2 - D_1^{-1}) - \mu_1^2(p^2 - D_2^{-1})}\,dp.$$

Finally, the substitutions $p = D_1^{-1/2}(1 + u^2)^{1/2}$ in the first integral and $p = D_2^{-1/2}(1 + u^2)^{1/2}$ in the second give

$$E_y(x, z = 0, t) = -\frac{1}{\pi^{3/2}t}\left(\frac{x^2}{T_1}\right)^{1/2}\exp(-x^2/T_1)\int_0^{\infty}\exp(-x^2u^2/T_1) \times \frac{\mu_1\mu_2^2u^2}{(\mu_2^2 - \mu_1^2)u^2 + \mu_1^2(D_1/D_2 - 1)}\,du + \frac{1}{\pi^{3/2}t}\left(\frac{x^2}{T_2}\right)^{1/2}\exp(-x^2/T_2)\int_0^{\infty}\exp(-x^2u^2/T_2) \times \frac{\mu_2\mu_1^2u^2}{(\mu_2^2 - \mu_1^2)u^2 + \mu_2^2(1 - D_2/D_1)}\,du. \quad (64)$$

This may not seem much of a simplification, but when the permeability is constant ($\mu_1 = \mu_2 = \mu_0$), the integrals on the right can be evaluated analytically. The result is

$$E_y(x, z = 0, t) = -\frac{1}{\pi x^2}\frac{1}{\sigma_2 - \sigma_1} \times [\exp(-x^2/T_1) - \exp(-x^2/T_2)]. \quad (65)$$

To our knowledge, this closed-form expression for the case when both half-spaces have a finite conductivity is new to the literature; it reduces to the known result for the case of air over a half-space of finite conductivity (Oristaglio 1982) on setting $\sigma_1 = 0$.

Similar expressions can be derived for the magnetic field at the interface. There is a complication, however, in that the inversion integrals are (formally) divergent, since they contain implicit delta-function contributions from the source. Proper treatment of these integrals is described in Appendix A. We obtain for H_x, the component parallel to the interface,

$$\{H_x^{(1)}, H_x^{(2)}\}(x, z = 0, t) = \frac{\{-\mu_2, \mu_1\}}{\mu_2 + \mu_1}\delta(x)H(t) - \left(\frac{1}{\pi^3 t}\right)^{1/2}\int_{D_1^{-1/2}}^{D_2^{-1/2}}\exp(-p^2x^2/4t) \times \mathrm{Im}\left[\frac{\mu_1\mu_2}{\mu_2 + \mu_1}\frac{-i(p^2 - D_1^{-1})^{1/2} - (D_2^{-1} - p^2)^{1/2}}{-\mu_2 i(p^2 - D_1^{-1})^{1/2} + \mu_1(D_2^{-1} - p^2)^{1/2}}\right]dp. \quad (66)$$

Note that the integral here is reduced to a finite range (see Appendix A), but there is no (obvious) closed-form simplification for the case $\mu_1 = \mu_2$. The component normal to the interface, H_z, is given by

$$\mu_1 H_z(x \ge 0, z = 0^-, t) = \mu_2 H_z(x \ge 0, z = 0^+, t) = -\left(\frac{1}{\pi^3 t}\right)^{1/2}\int_{D_1^{-1/2}}^{\infty}\exp(-p^2x^2/4t) \times \frac{\mu_1\mu_2^2(p^2 - D_1^{-1})^{1/2}}{\mu_2^2(p^2 - D_1^{-1}) - \mu_1^2(p^2 - D_2^{-1})}p\,dp + \left(\frac{1}{\pi^3 t}\right)^{1/2}\int_{D_2^{-1/2}}^{\infty}\exp(-p^2x^2/4t) \times \frac{\mu_1^2\mu_2(p^2 - D_2^{-1})^{1/2}}{\mu_2^2(p^2 - D_1^{-1}) - \mu_1^2(p^2 - D_2^{-1})}p\,dp. \quad (67)$$

For $\mu_1 = \mu_2 = \mu_0$, this reduces to

$$H_z(x \geq 0, z = 0, t) = -\frac{2t}{\pi x^3}\frac{D_2 D_1}{D_1 - D_2} \times [\exp(-x^2/T_1) - \exp(-x^2/T_2)]. \quad (68)$$

Finally, $H_z(x \leq 0) = -H_z(x \geq 0)$.

7 NUMERICAL EXAMPLES

In evaluating numerically the general expressions for the fields in the two half-spaces, further manipulation of the integrals is useful. The manipulations, described in Appendix B, are designed to reduce the range of integration to a standard form that is independent of the point of observation and to subtract the asymptotic behaviour of the integrand (as the integration variable goes to infinity) in order to improve numerical convergence. After these manipulations, we obtain for E_y, the electric field in the more diffusive domain $\mathcal{D}_1$,

$$E_y^{(1)}(x, z, t) = -\frac{1}{2\pi}\frac{\mu_2}{\mu_2 + \mu_1}\frac{\mu_1}{t}\exp(-r^2/T_1) + \frac{1}{\pi^{3/2}}\frac{\mu_1}{t}\left(\frac{r^2}{T_1}\right)^{1/2}\exp(-r^2/T_1) \times \int_0^\infty \exp(-r^2 v^2/T_1)\,\mathrm{Re}\left(\frac{\mu_2}{\mu_1 + \mu_2} - \frac{\mu_2 \bar{\gamma}_1}{\mu_2 \bar{\gamma}_1 + \mu_1 \bar{\gamma}_2}\right) dv, \quad (69)$$

where now

$$p_1 = (\sigma_1 \mu_1)^{1/2}\left[\frac{x}{r}(v^2 + 1)^{1/2} + i\frac{|z|}{r}v\right] \quad (70)$$

and

$$\bar{\gamma}_1 = (\sigma_1 \mu_1 - p_1^2)^{1/2}. \quad (71)$$

$$\bar{\gamma}_2 = (\sigma_2 \mu_2 - p_1^2)^{1/2}, \quad (72)$$

as before.

The direct-wave part of electric field in the less diffusive

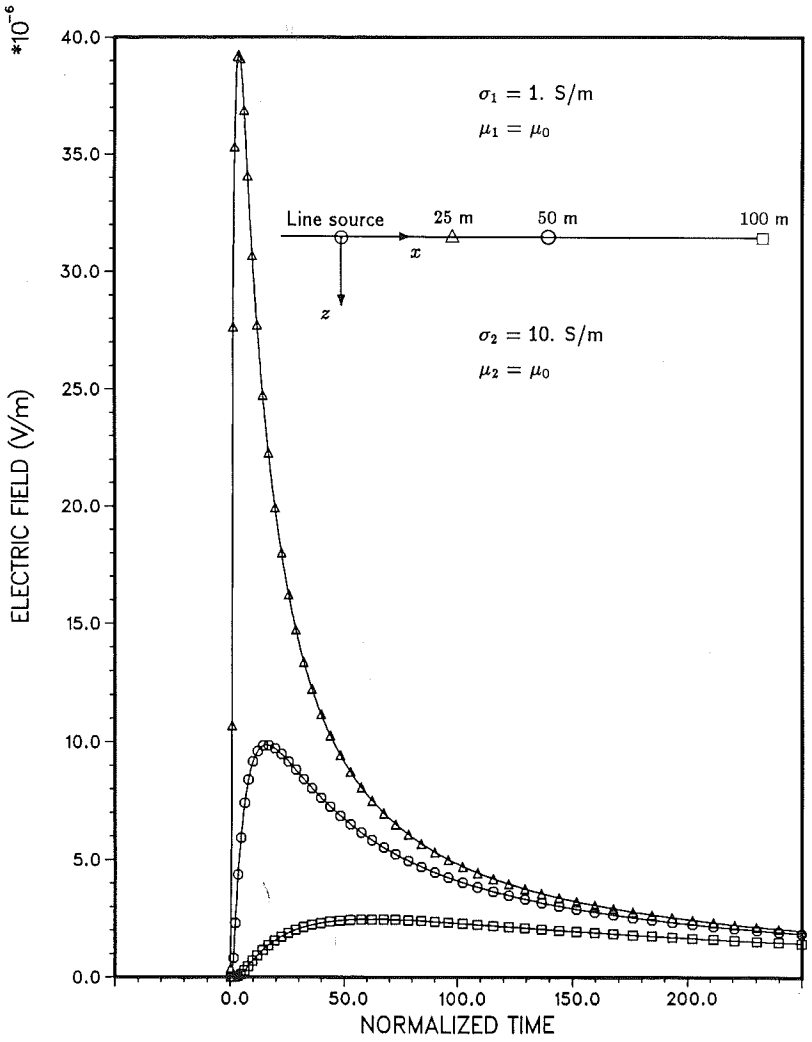

Figure 4. Electric field at the interface between two half-spaces following shut-off of a steady current of 1 A in a line-source at the interface: analytical solution (solid lines) and results obtained by numerical integration of the general expression derived by the modified Cagniard method (symbols). Field values are shown as a function of time at three distances from the source. Time is normalzed by $T = 4t/\sigma_1 \mu_1 r^2$, where t is the time in s, and $r = 25$ m.

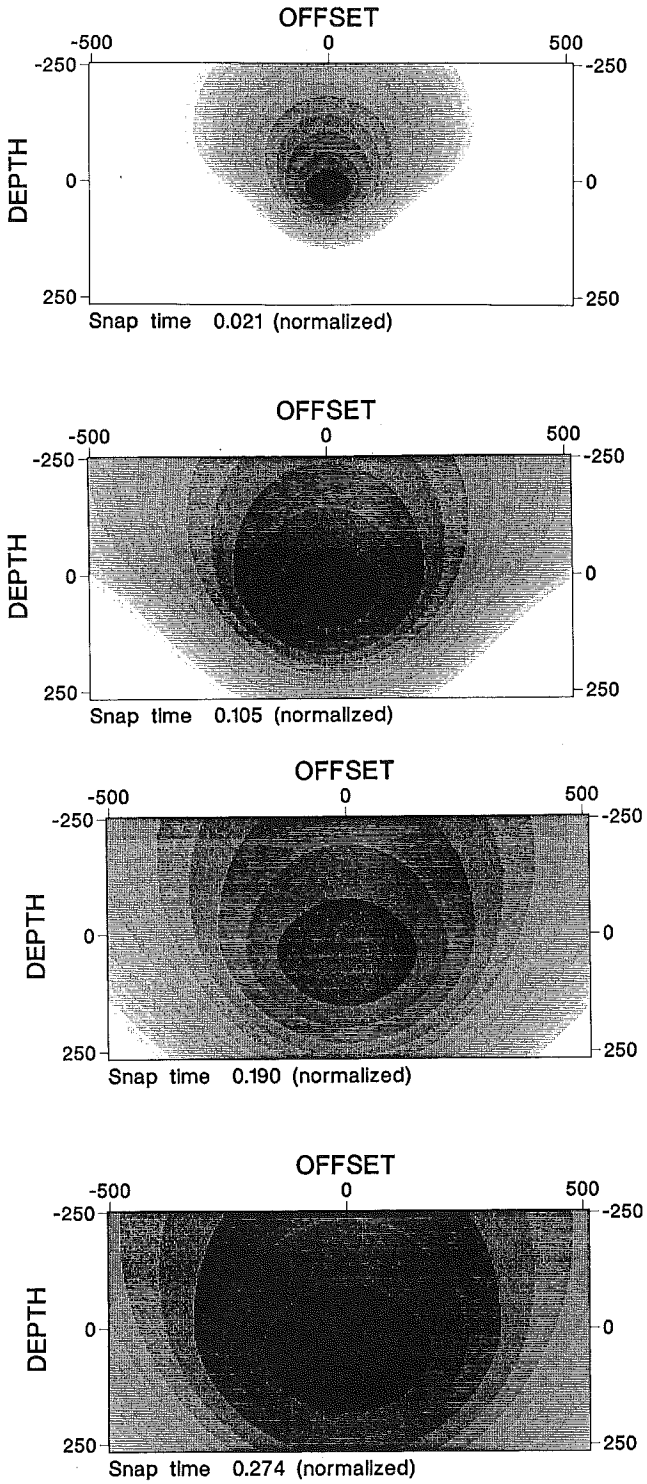

Figure 5. Four snapshots showing the evolution of the electric field in two half-spaces following shut-off of a steady current of 1 A in a line-source at the interface, $(x, z) = (0, 0)$. Medium properties are the same as in Fig. 4. Each plot is normalized by the maximum of the electric field at the corresponding time; grey levels are logarithmic, decreasing by the factor 0.8 between successive levels. Time is normalized by $T = 4t/\sigma_1\mu_1 r^2$, where t is the time in s, and $r = 560$ m.

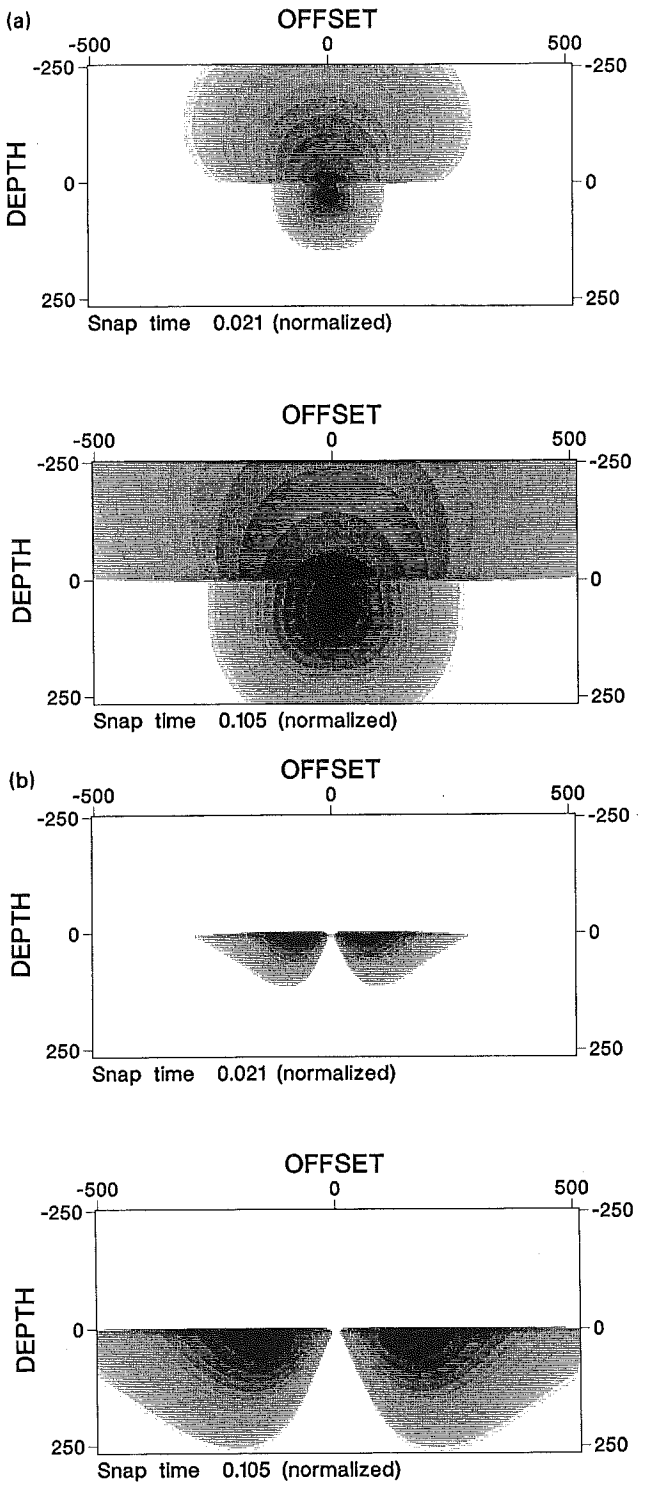

Figure 6. (a) Two snapshots of the electric field in two half-spaces following shut-off of a steady current of 1 A in a line-source at the interface, $(x, z) = (0, 0)$. The head-wave contribution to the field in the lower half-space is omitted. Medium properties are the same as in Fig. 4. Each plot is normalized by the maximum of the electric field at the corresponding time; grey levels are logarithmic, decreasing by the factor 0.8 between successive levels. Time is normalized by $T = 4t/\sigma_1\mu_1 r^2$, where t is the time in s, and $r = 560$ m. (b) Head-wave contributions corresponding to the snapshots in (a). Adding these contributions to the fields shown in (a) gives the total field shown in Fig. 5.

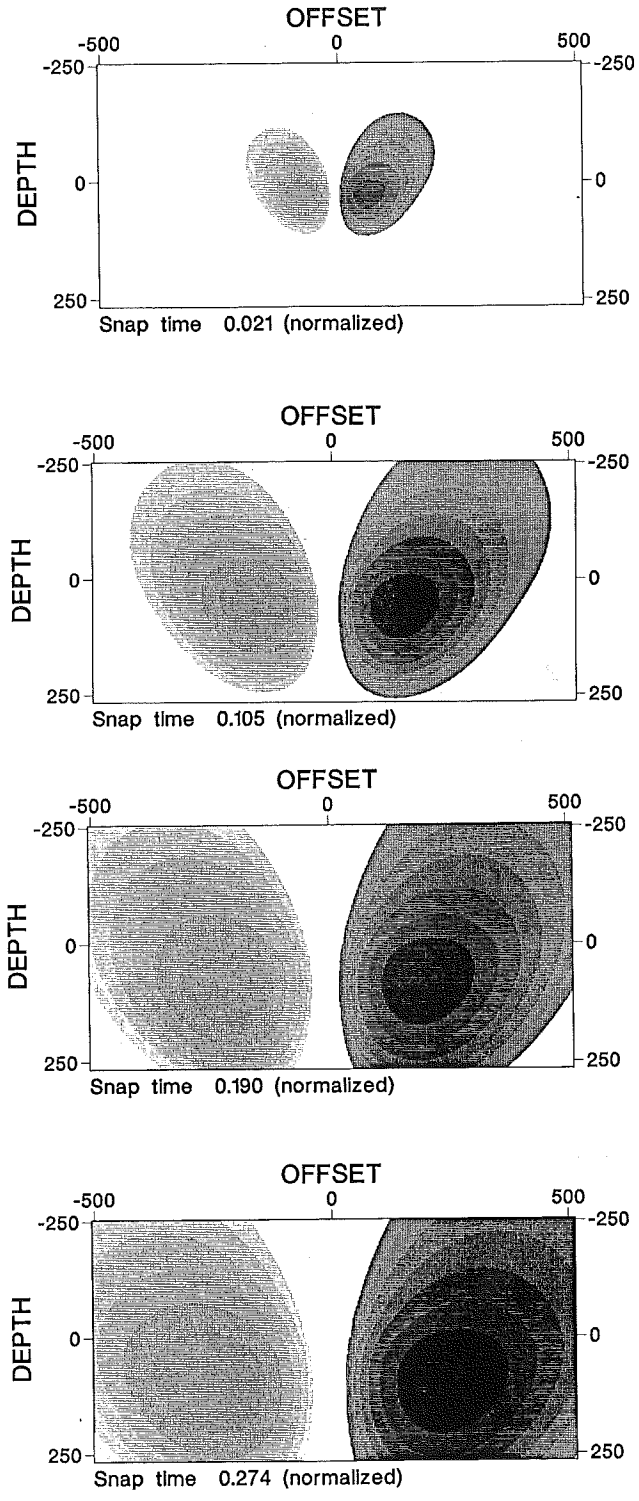

Figure 7. Four snapshots showing the evolution of the electric field in two half-spaces following shut-off of steady currents of ±1 A in two line-sources at the interface, with the positive source at $(x, z) = (0, 0)$ and the negative source at $(x, z) = (-10, 0)$. Medium properties are the same as in Fig. 4. Each plot is normalized by the maximum of the electric field at the corresponding time; grey levels are logarithmic, decreasing (in absolute value) by the factor 0.8 between successive levels. The lighter-grey levels on the left represent negative values. Time is normalized by $T = 4t/\sigma_1\mu_1 r^2$, where t is the time in s, and $r = 560$ m.

domain $\mathcal{D}_2$ can be obtained from (69) by permuting the subscripts 1 and 2. The head-wave contribution in the region $(D_1/D_2)^{1/2} < x/r \leq 1$ is given by

$$E_y^{(HW)}(x, z, t) = -\frac{1}{\pi^{3/2}}\frac{\mu_2}{t}\left(\frac{r^2}{T_2}\right)^{1/2}\exp(-r^2/T_2) \times \int_0^{v_{2,1}} \exp(r^2v^2/T_2)\,\mathrm{Im}\left(\frac{\mu_1\bar{\gamma}_2}{\mu_2\bar{\gamma}_1 + \mu_1\bar{\gamma}_2}\right) dv, \quad (73)$$

where

$$\bar{\gamma}_1 = (\sigma_1\mu_1 - p_{2,1}^2)^{1/2}, \quad (74)$$

$$\bar{\gamma}_2 = (\sigma_2\mu_2 - p_{2,1}^2)^{1/2}, \quad (75)$$

and

$$p_{2,1} = (\sigma_2\mu_2)^{1/2}\left[\frac{x}{r}(1 - v^2)^{1/2} - \frac{z}{r}v\right], \quad (76)$$

$$v_{2,1} = \left(1 - \frac{\sigma_1\mu_1}{\sigma_2\mu_2}\right)^{1/2}\frac{x}{r} - \left(\frac{\sigma_1\mu_1}{\sigma_2\mu_2}\right)^{1/2}\frac{z}{r}. \quad (77)$$

As a first example (Fig. 4), we consider the electric field at the interface between half-spaces with conductivities $\sigma_1 = 1\ \mathrm{S\,m^{-1}}$ and $\sigma_2 = 10\ \mathrm{S\,m^{-1}}$. The permeability in both half-spaces is the free-space value. The figure compares the analytical values for the field, obtained from (65), with those obtained by numerical integration of the general expression (69) using a simple trapezoidal rule. Agreement between the analytical and numerical values seems to be satisfactory. The electric field was computed at 250 time-points for each of the three curves, corresponding to different distances from the source. The total computation took about 1 min of CPU time on a VAX 8600.

Figures 5 and 6 illustrate the development of the diffusive head wave. Fig. 5 shows a sequence of four snapshots of the total electric field in the two half-spaces. Fig. 6(a) shows the electric field minus the head-wave contribution for the first two snapshots of Fig. 5; Fig. 6(b) shows the corresponding head waves. As with a true head wave, the diffusive head wave in the 'slow' medium—here, the lower half-space with a smaller diffusion coefficient than the upper half-space—is induced by the rapid spread of the field in the fast medium. Physically, it is required in order to maintain the continuity of the electric field across the interface.

The final example (Fig. 7) shows snapshots of the electric field when two line-sources of opposite polarity are placed at the interface, as in 2-D simulation of a finite-loop source. Even with a finite conductivity in the upper half-space, the familiar (2-D) smoke-ring pattern develops, with positive and negative concentrations of current arising near the two limbs of the source and diffusing diagonally downward into the bottom half-space as time progresses.

8 DISCUSSION AND CONCLUSIONS

We have illustrated the application of Cagniard's method to (electromagnetic) diffusion problems in the canonical example of a line-source situated at the interface between two conductive media. With this method, space–time expressions for the field values anywhere in the configuration are obtained in the form of well-behaved integrals.

When only the conductivity varies across the interface, the integral expression for the electric field at the interface can be obtained in closed form; but the general expressions themselves are also readily computed by numerical integration. Even for this simple configuration, this method provides physical insight into the behaviour of the field by isolating the contributions of the direct waves from a diffusive head wave that develops along the interface and propagates into the less diffusive medium.

The ideas developed here can easily be extended to deal with multilayered media or 3-D sources. The extensions required are mainly in the form of book-keeping and follow the lines of the 'generalized ray method' that is used for the problems of impulsive wave propagation in layered media. These extensions will be treated in subsequent papers.

ACKNOWLEDGMENTS

This work was carried out while the first author (A.T.d.H.) was on leave of absence from Delft University of Technology, Department of Electrical Engineering, Laboratory of Electromagnetic Research, and was a visiting scientist at Schlumberger Doll Research, Ridgefield, Connecticut, USA (April 1985) and at Etudes et Productions Schlumberger, Clamart, France (March 1986).

REFERENCES

Achenbach, J. D., 1973. *Wave Propagation in Elastic Solids,* North-Holland, Amsterdam.

Aki, K. & Richards, P. G., 1980. *Quantitative Seismology,* W. H. Freeman, San Francisco.

De Hoop, A. T., 1960. A modification of Cagniard's method for solving seismic pulse problems, *Appl. Sci. Res.,* **B8,** 349–356.

De Hoop, A. T., 1961. Theoretical determination of the surface motion of a uniform elastic half-space produced by a dilatational, impulsive, point source, *Proc. Colloque International C.N.R.S.,* No. 111, Marseille, 21–32.

De Hoop, A. T., 1979. Pulsed electromagnetic radiation from a line source in a two-media configuration, *Radio Sci.,* **14,** 253–268.

De Hoop, A. T. & Van der Hijden, J. H. M. T., 1983. Generation of acoustic waves by an impulsive line source in a fluid/solid configuration with a plane boundary, *J. acoust. Soc. Am.,* **74,** 333–342.

De Hoop, A. T. & Van der Hijden, J. H. M. T., 1984. Generation of acoustic waves by an impulsive point source in a fluid/solid configuration with a plane boundary, *J. acoust. Soc. Am.,* **75,** 1709–1715.

Edwards, R. N. & Cheesman, S. J., 1987. Two-dimensional modelling of a towed magnetic dipole–dipole sea floor EM system, *J. Geophys.,* **61,** 110–121.

Goldman, M. M. & Stoyer, C. H., 1983. Finite difference calculations of the transient field of an axially symmetric earth for vertical magnetic dipole excitation, *Geophysics,* **48,** 953–963.

Inan, A. S., Fraser-Smith, A. C. & Villard, O. G., Jr, 1986. ULF/VLF electromagnetic fields generated along the seafloor interface by a straight current source of infinite length, *Radio Sci.,* **21,** 409–420.

King, R. W. P., 1985. Electromagnetic surface waves: New formulas and their application to determine the electrical properties of the sea bottom, *J. Appl. Phys.,* **58,** 3612–3624.

Kuo, J. T. & Cho, D.-H., 1980. Transient time-domain electromagnetics, *Geophysics,* **45,** 271–291.

McCracken, K. G., Oristaglio, M. L. & Hohmann, G. W., 1986. A comparison of electromagnetic exploration systems, *Geophysics,* **51,** 810–818.

Nabighian, M. N., 1979. Quasi-static transient response of a conducting half-space: An approximate representation, *Geophysics,* **44,** 1700–1705.

Oristaglio, M. L., 1982. Diffusion of electromagnetic fields into the earth from a line source of current, *Geophysics,* **47,** 1585–1592.

Oristaglio, M. L. & Hohmann, G. W., 1984. Diffusion of electromagnetic fields into a two-dimensional earth: A finite-difference approach. *Geophysics,* **49,** 870–894.

APPENDIX A. TREATMENT OF SINGULAR INTEGRALS

In the expressions for the magnetic field at the interface, divergent integrals arise, which could be expected from the presence of the (spatial) delta-function source. This appendix describes the proper treatment of these integrals. We begin with the transform domain expressions for H_x at the interface, which follow from (18) and (21) on putting $z = 0$,

$$\hat{H}_x^{(1)} = -\frac{s^{-1/2}}{2\pi i}\int_{-i\infty}^{i\infty} \exp(-s^{1/2}px)\bar{\gamma}_1\mu_1^{-1}\bar{A}(p)\,dp \tag{A1}$$

and

$$\hat{H}_x^{(2)} = \frac{s^{-1/2}}{2\pi i}\int_{-i\infty}^{i\infty} \exp(-s^{1/2}px)\bar{\gamma}_2\mu_2^{-1}\bar{A}(p)\,dp. \tag{A2}$$

To extract the correct interpretation of these integrals, we observe that

$$\bar{\gamma}_1\mu_1^{-1}\bar{A}(p) \sim \frac{\mu_2}{\mu_1+\mu_2} \quad \text{as } |p|\to\infty \tag{A3}$$

and

$$\bar{\gamma}_2\mu_2^{-1}\bar{A}(p) \sim \frac{\mu_1}{\mu_1+\mu_2} \quad \text{as } |p|\to\infty. \tag{A4}$$

Furthermore, we have

$$\frac{s^{1/2}}{2\pi i}\int_{-i\infty}^{i\infty} \exp(-s^{1/2}px)\,dp = \delta(x). \tag{A5}$$

With this, (A1) and (A2) can be re-written as

$$\hat{H}_x^{(1)} = -\frac{\mu_2}{\mu_1+\mu_2}s^{-1}\delta(x) - \frac{s^{-1/2}}{2\pi i} \times \int_{-i\infty}^{i\infty} \exp(-s^{1/2}px)\bar{B}(p)\,dp \tag{A6}$$

and

$$\hat{H}_x^{(2)} = \frac{\mu_1}{\mu_1+\mu_2}s^{-1}\delta(x) - \frac{s^{-1/2}}{2\pi i} \times \int_{-i\infty}^{i\infty} \exp(-s^{1/2}px)\bar{B}(p)\,dp, \tag{A7}$$

where

$$\bar{B}(p) = \frac{\mu_1\mu_2(\bar{\gamma}_1-\bar{\gamma}_2)}{(\mu_1+\mu_2)(\mu_2\bar{\gamma}_1+\mu_1\bar{\gamma}_2)}. \tag{A8}$$

Since $|B|\to 0$ as $|p|\to\infty$, the integrands in the above equations satisfy the conditions of Jordan's lemma. Applying the contour deformations as described in the text

gives

$$H_x^{(1)} = -\frac{\mu_2}{\mu_1+\mu_2}\delta(x)H(t) - \frac{1}{\pi}\int_{D_1^{-1/2}}^{\infty} F(t, px)\,\mathrm{Im}\,[\bar{B}(p)]\,dp \quad \text{(A9)}$$

and

$$H_x^{(2)} = +\frac{\mu_1}{\mu_1+\mu_2}\delta(x)H(t) - \frac{1}{\pi}\int_{D_1^{-1/2}}^{\infty} F(t, px)\,\mathrm{Im}\,[\bar{B}(p)]\,dp. \quad \text{(A10)}$$

Finally, we note that $\mathrm{Im}\,[\bar{B}(p)]$ is identically zero for $p > D_2^{-1/2}$, which reduces these expressions to the finite-range integrals given in the text (equation 66).

For H_z, the component normal to the interface, we start with

$$\hat{H}_z^{(1)} = -\frac{s^{-1/2}}{2\pi i}\int_{-i\infty}^{i\infty} \exp(-s^{1/2}px)p\mu_1^{-1}\bar{A}(p)\,dp \quad \text{(A11)}$$

and

$$\hat{H}_z^{(2)} = -\frac{s^{-1/2}}{2\pi i}\int_{-i\infty}^{i\infty} \exp(-s^{1/2}px)p\mu_2^{-1}\bar{A}(p)\,dp. \quad \text{(A12)}$$

In this case, since

$$\bar{A}(p) \sim \frac{\mu_1\mu_2}{\mu_1+\mu_2}(\pm ip) \quad \text{as } |p|\to\infty \qquad \mathrm{Im}\,(p) \gtrless 0, \quad \text{(A13)}$$

the integrals' Cauchy principal values around infinity exist, which is the proper way to interpret them physically. On applying the contour deformations described in the text, we note that the contributions from the joining circular arcs at infinity *cancel* in view of (A13) (Jordan's lemma does not apply in this case). We thus arrive at

$$H_z^{(1)} = -\frac{1}{\pi}\int_{D_1^{-1/2}}^{\infty} F(t, px)p\mu_1^{-1}\,\mathrm{Im}\,[\bar{A}(p)]\,dp \quad \text{(A14)}$$

and

$$H_z^{(2)} = -\frac{1}{\pi}\int_{D_1^{-1/2}}^{\infty} F(t, px)p\mu_2^{-1}\,\mathrm{Im}\,[\bar{A}(p)]\,dp. \quad \text{(A15)}$$

APPENDIX B. NUMERICAL EVALUATION OF THE INTEGRALS

In this Appendix, we reduce the integral expressions for the field components to a convenient form for numerical integration. Our reduction is surely not unique, but it leads to a reasonably fast, accurate, and simple numerical algorithm. Since all the integrals are similar, we describe the steps in detail for just the electric field component $E_y^{(1)}$, given by (37). Writing this equation out explicitly, we have

$$E_y^{(1)}(x, z, t) = -\frac{1}{2(\pi t)^{3/2}}\int_{\kappa_1}^{\infty} \kappa \exp(-\kappa^2/4t) \times \mathrm{Im}\left[\frac{\mu_1\mu_2}{\mu_2\bar{\gamma}_1+\mu_1\bar{\gamma}_2}\frac{i\bar{\gamma}_1}{(\kappa^2-\kappa_1^2)^{1/2}}\right] d\kappa. \quad \text{(B1)}$$

where

$$\kappa_1 = (\sigma_1\mu_1 r^2)^{1/2},$$

$$\bar{\gamma}_1 = \kappa\frac{|z|}{r^2} - i(\kappa^2-\kappa_1^2)^{1/2}\frac{x}{r^2},$$

$$\bar{\gamma}_2 = (\sigma_2\mu_2 - \sigma_1\mu_1 + \bar{\gamma}_1^2)^{1/2}.$$

Introducing the dimensionless variable k by the substitution

$$\kappa = (\sigma_1\mu_1 r^2)^{1/2}k$$

makes the range of integration run from 1 to ∞, independent of r. This and some simple rearranging give

$$E_y^{(1)}(x, z, t) = -\frac{\mu_1}{\pi^{3/2}t}\left(\frac{r^2}{T_1}\right)^{1/2}\int_1^{\infty}\frac{k}{(k^2-1)^{1/2}} \times \exp(-k^2r^2/T_1)\,\mathrm{Re}\left(\frac{\mu_2\bar{\gamma}_1}{\mu_2\bar{\gamma}_1+\mu_1\bar{\gamma}_2}\right) dk, \quad \text{(B2)}$$

where $T_1 = 4t/\sigma_1\mu_1$ is the scaled time variable.

The singularity at $k = 1$ (integrable but bothersome numerically) is then removed by the substitution

$$v = (k^2-1)^{1/2},$$

giving

$$E_y^{(1)}(x, z, t) = -\frac{\mu_1}{\pi^{3/2}t}\left(\frac{r^2}{T_1}\right)^{1/2}\exp(-r^2/T_1) \times \int_0^{\infty}\exp(-v^2r^2/T_1)\,\mathrm{Re}\left(\frac{\mu_2\bar{\gamma}_1}{\mu_2\bar{\gamma}_1+\mu_1\bar{\gamma}_2}\right) dv, \quad \text{(B3)}$$

The last step is to subtract off the asymptotic behaviour of the integrand, using

$$\frac{\mu_2\bar{\gamma}_1}{\mu_2\bar{\gamma}_1+\mu_1\bar{\gamma}_2} \to \frac{\mu_2}{\mu_2+\mu_1} \quad \text{as } v\to\infty.$$

The final expression is then

$$E_y^{(1)}(x, z, t) = -\frac{1}{2\pi}\frac{\mu_2}{\mu_2+\mu_1}\frac{\mu_1}{t}\exp(-r^2/T_1) + \frac{1}{\pi^{3/2}}\frac{\mu_1}{t} \times \left(\frac{r^2}{T_1}\right)^{1/2}\exp(-r^2/T_1)\int_0^{\infty}\exp(-r^2v^2/T_1) \times \mathrm{Re}\left(\frac{\mu_2}{\mu_1+\mu_2} - \frac{\mu_2\bar{\gamma}_1}{\mu_2\bar{\gamma}_1+\mu_1\bar{\gamma}_2}\right) dv. \quad \text{(B4)}$$